

Density fluctuation measurement using Rayleigh scattering

Bertrand Mercier⁽¹⁾, Emmanuel Jondeau⁽¹⁾, Thomas Castelain⁽²⁾, Christophe Bailly⁽¹⁾

⁽¹⁾Laboratoire de Mécanique des fluides et d'Acoustique, École Centrale de Lyon & UMR CNRS 5509,
36 av. Guy de Collongue, 69134 Écully France, bertrand.mercier@doctorant.ec-lyon.fr

⁽²⁾Univ Lyon, Université Lyon 1, LMFA UMR CNRS 5509, 36 av. Guy de Collongue, 69134 Écully France

ABSTRACT

A Rayleigh scattering based system intended for measuring flow density is set-up in an anechoic wind tunnel. This measurement method is non-intrusive and offers an attractive perspective for aeroacoustic applications. The results provided by the present bench agree well with theoretical expectations in clean air, but a high sensitivity to the presence of dust particles in the flow is encountered. The wind tunnel is therefore equipped with an air filter. A post-processing method is also applied to clean up signals from dust particle detections. Mean and fluctuating density profiles are measured in a Mach 0.9 jet. The strong influence of the shot noise that is intrinsic to this measurement technique, is pointed out. A method using a single light-sensor is developed to reduce this suprious noise, and results are compared with the Panda and Seasholtz [11] method that requires two sensors.

1. INTRODUCTION

Aeroacoustic studies generally involve high speed flow and large scale facilities. Beside this first consideration, measurement techniques must be as non-intrusive as possible for preventing the generation of any spurious sound induced by the flow alteration. Instrumentation systems that comply with these restrictions are limited in variety. Statistical flow properties can be obtained through PIV (Particle Image Velocitmetry) or LDV (Laser Doppler Velocitmetry) which are generally not considered as intrusive [14, 4, 3, 1]. Nevertheless, they require the use of seed particles of which inertia introduces biases when measuring flow containing high normal or shear stresses. Even though those issues can be partially avoided by correction procedures, they are in general not well enough time-resolved for high speed flow, and therefore not eligible for problems requiring time series such as cross-correlation computations. Optical deflectometry based techniques are other approaches that do not require any flow seeding, and that can be sampled at high frequency.

In spite of these properties, an intrinsic spatial integration prevents from quantitative investigations of turbulent flows.

Rayleigh scattering based methods are alternative techniques which can meet all the above-mentioned requirements. These methods rest upon the analysis of laser light scattered by the molecules that constitute the flow, thus no seeding is needed. In principle, the intensity of the scattered light is linearly related to the local flow density, and the spectral analysis of this light makes the measurement of the local temperature, and velocity achievable. These two approaches can either be time resolved, or not. Examples of time-resolved density measurements are given in [13, 16, 11, 12, 8, 9], and spectral analysis in [17, 5, 6].

The present study focuses on density measurements, the spectrum of the light will not be analysed. The objective is to describe the validation process of a new Rayleigh scattering bench. After the Rayleigh scattering theoretical aspects are described, the experimental setup, and the specificity of this particular bench concerning data acquisition will be discussed. Then, the validity of the measurement system will be analysed though some validation tests, and some results will be provided in a final section.

2. RAYLEIGH SCATTERING THEORY

Rayleigh scattering is a process whereby light is scattered by particles much smaller than the wavelength of the incident light. For the measurement of air density, the scattering particles are the molecules contained in air, and the incident light source is a linearly polarised laser beam. If the laser wavelength λ is in the visible range, the particles are about thousand times smaller than λ which fully meet the hypothesis.

This light scattering process is commonly referred to as an elastic process, involving no loss of energy in terms of electromagnetic radiation. However, the scattered part of the energy is spread on a spectrum wider than the inci-

dent one. This broadening mostly depends on the temperature for a given type of particle. The motion of the particles relative to the observer also introduces a Doppler shift onto the spectrum. These two effects are described in more details in [7], and in [18] with historical perspectives. They allow throughout a spectrum analysis for measuring the temperature and the bulk velocity of the gas in the probed volume. The measure of density rests upon the power of the light P_s scattered by a volume of gas, in comparison to the incident power. P_s is actually the net power resulting from the contribution of all individual molecules, and is therefore related to their concentration, hence to the density. Otherwise, the power scattered by a single molecule P_s^i undergoing a laser beam of intensity I_i in W/m^2 , into a solid angle $\partial\Omega$, and with an angle ϕ between the observer and the electric field of the incident light, can be calculated by introducing a differential scattering cross section $\partial\sigma/\partial\Omega$

$$P_s^i = \frac{\partial\sigma}{\partial\Omega} \partial\Omega \sin^2(\Phi) I_i \quad (1)$$

The differential scattering cross section is specific to a given type of particle, and may depend upon the direction of observation with respect to the beam path for a non spherical particle. The total power scattered into $\partial\Omega$ can be calculated as the sum of all individual contributions. For a gas of numeric density N and a probed volume V_{sc} , P_s is given by

$$P_s = N V_{sc} \frac{\partial\sigma}{\partial\Omega} \partial\Omega \sin^2(\Phi) I_i \quad (2)$$

and the numeric density N of a gas of density ρ and molecular mass M is

$$N = \frac{\rho N_A}{M} \quad (3)$$

where N_A is the Avogadro constant.

The scattered power P_s is finally written as

$$P_s = \frac{\rho N_A}{M} V_{sc} \frac{\partial\sigma}{\partial\Omega} \partial\Omega \sin^2(\Phi) I_i \quad (4)$$

Noting that the energy of a photon is hc/λ , with h the Planck constant, and c the speed of light, the scattered power can be turned into a photon flux. By taking into account the quantum efficiency of the photo-sensor Q_E which corresponds to the ratio of the number of detected photons by the number of all incoming photons, the flux of detected photons Φ_d in photons/s is

$$\Phi_d = Q_E \frac{\lambda}{hc} \frac{N_A}{M} \frac{\partial\sigma}{\partial\Omega} \partial\Omega V_{sc} \rho \sin^2(\Phi) I_i \quad (5)$$

This equation highlights the linear relation between the detected photon flux and the density. Therefore, the density can be deduced by measuring the photon flux.

It is possible to estimate the flux expected for the parameters of this study, and by assuming air is made of 20% of oxygen, and 80% of nitrogen. The differential scattering cross section of air is calculated from the sum of the differential scattering cross sections of oxygen and nitrogen weighted by the molecular fraction. These values are

λ	532	nm
$\partial\Omega$	3.1×10^{-2}	sr
V_{sc}	2.3×10^{-10}	m^3
I_i	3.8×10^6	W/m^2
$\partial\sigma/\partial\Omega$	5.9×10^{-32}	m^2/Sr
$N_A/(hcM)$	1.0×10^{50}	$\text{J}^{-1} \text{m}^{-1} \text{kg}^{-1}$
Φ	$\pi/2$	rad
Q_E	0.4	

Table 1: Typical value of the Rayleigh scattering bench required for estimating the photon flux (5).

provided in [15], and summarized up in table 1 with the other required quantities. For a density of 1.2 kg/m^3 , Φ_d

$$\Phi_d = 4.2 \times 10^7 \text{ photon/s} \quad (6)$$

This estimation is valid for pure air, but is almost not influenced by other contaminants such as water vapour because it represents a very small mass fraction. However, as soon as vapour condenses to form droplets, the Rayleigh theory cannot handle any more such large particles, and Mie theory must be employed instead. This large diameter is associated with a drastic increase of the scattering cross section, so the flux of photons will be increased in the same proportion. The same event occurs when a dust particle passes across the probed volume. As an example, after Mie theory, a spherical particle of diameter $1 \mu\text{m}$ scatters hundred times more light than all molecules of the probed volume.

3. EXPERIMENTAL SET-UP

The Rayleigh scattering bench here presented is designed to operate in the anechoic wind tunnel of the Centre for Acoustics in École Centrale de Lyon. This room is acoustically treated by using glass fibre, so the dust concentration is high inside. That is not really compatible with Rayleigh scattering measurement requiring air as clean as possible. This problem is avoided by using a coaxial wind tunnel shown in Fig. 1. An inner nozzle of 38 mm in diameter is fed by a compressor equipped with an air dryer. An outer nozzle of 200 mm in diameter is used at low speed to provide a clean environment for the jet to develop in. These two air supplies are equipped with HEPA air filters. The measurement system is mainly composed by a 532 nm continuous 5 W laser, a collecting optic and a beam dump. In addition, the laser beam passes across a half-wave plate which makes possible rotating the electric field direction. A plane mirror is also used to direct the beam toward the desired direction. The light scattered in the probe region is collected by a 160 mm diameter and 750 mm focal length lens. A second convergent lens focus the light toward a 1 mm by 200 μm slit which delimit a cylindrical probed volume of diameter 1.5 mm and height 0.3 mm. A photomultiplier is installed behind the slit to convert light intensity into electric signal. The acquisition system is a major advancement of this system in comparison with ones already described in the literature. This point is therefore discussed in detail in the next

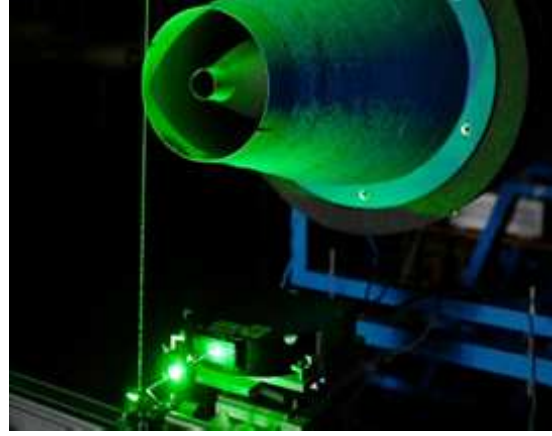
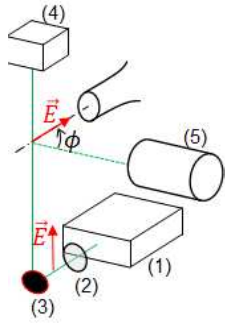


Figure 1: Schematics of the Rayleigh scattering system, and the corresponding photography. (1) Laser head, (2) half-wave plate, (3) mirror, (4) beam dump, (5) collecting optic. \vec{E} denote the electric field direction.

section.

4. DATA ACQUISITION

4.1 Data-acquisition chain

The first element of the data-acquisition chain is a photomultiplier which converts the collected light flux into an electric signal. Many types of photomultiplier exist, and can first be categorised as voltage and current output types. Voltage output types contain a built-in transimpedance amplifier that limit the bandwidth of the sensors. These sensors are used to measure an analog voltage signal representative of the light intensity. Current output types sensors are in general faster and are suitable for single photon counting, which is useful for measuring very low light intensity. In this mode, each detected photon is converted into a short current pulse. A Hamamatsu H7422P-40 type photomultiplier is selected for its short rise time of 1 ns and its fairly high gain of 10^6 , meaning one photon detection turns into a 10^6 electrons pulse. The pulses are then counted to estimate the photon flux, hence the density from Eq. (5). In all Rayleigh scattering systems of our knowledge, the output of the photomultiplier is connected to a photon-counter, via a transimpedance amplifier if needed. These devices are set to count the number of photon-detections in successive time windows of a predetermined duration Δt to generate a time series of the photon flux at a frequency $f_{acq} = 1/\Delta t$. However, a dead time, known as pulse pair resolution τ , arises after all photon counting, which prevents for counting another photon during this period of typically 5 to 25 ns (models Stanford Research SR400 and Hamamatsu C9744). The pulse pair resolution becomes a problem when the photon flux increases, because the probability for two detections to be spaced by less than the pulse pair resolution increases. This introduces a non-linearity between the counted photon flux Φ and the detected photon flux Φ_d . Besides, an intrinsic uncertainty comes out when counting photons. This is the so-called shot noise that results from the randomness of photon time arrival. This ran-

domness is governed by a Poisson law, so the properties of such a law apply on the number of counted photons. The relevant property is the equality between the photon counted from a fixed flux and the variance of this number. This leads to define a floor of the signal to noise ratio equal to $1/\sqrt{\Phi_d \Delta t}$, thus the photon flux should be maximized.

According to these constraints, the choice of not using such a photon-counter is made. Instead, the photomultiplier output signal is digitised directly, and the photon counting is performed from time series of this signal during post-processing. The digitiser is chosen to be able to digitise few millivolt signals at a rate high enough to capture 2 ns pulses. The National Instrument high speed PXIe 5160 meets all the specifications, and is therefore chosen. The maximum sampling rate of this system is 2.5 GHz, with a cut-off frequency of 500 MHz. But to improve the record length, it is limited to 1.25 GHz for maximum 0.86 s records. The pulse pair resolution of this system has been estimated from measurement to be 2 ns, that is a limitation attributable to the pulse width.

4.2 Photon flux estimation

The estimation of the time evolution of the photon flux is performed by counting the number of photons detected during successive time intervals. The length of these intervals defines the sampling frequency of the flux. The first step of this process is to define a way of identifying the signature of photon detections in the digitised photomultiplier output. An example of a digitised signal is provided in Fig. 2. The detection signature demarcates well from the electronic noise. The identification of photon arrival is therefore simply done by marking the local maximum of the signal that are greater than a threshold. The date of arrival of each photon is then stored in a tabular. At this point no sampling frequency has been defined, and that is a major advantage of this counting technique in comparison with commercial counter way. Since all photon detections are indexed, it is straightforward to define a desired sampled frequency and to allocate the detected photons into the right bin.

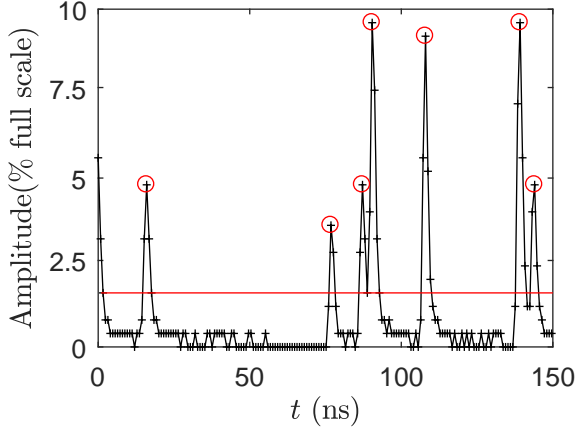


Figure 2: Time series of the photomultiplier output signal digitized at 1.25 GHz. The red solid line indicates the noise threshold and red circles marks the counted photons.

It is mentioned in the previous section that there is a deficit of counted photon flux Φ in comparison to detected photon flux Φ_d due to the pulse pair resolution of the system. The relation between these two values can be determined since the probability to detect a photon within a time interval dt follows a Poisson law of parameter $\Phi_d dt$, therefore, the probability of detecting n photons during dt is

$$p(n, dt) = \frac{(\Phi_d dt)^n}{n!} e^{-\Phi_d dt} \quad (7)$$

and the probability for counting a photon is equal to the probability of detecting no photon during the pulse pair resolution $p(0, \tau)$

$$\Phi = \Phi_d p(0, \tau) = \Phi_d e^{-\Phi_d \tau} \quad (8)$$

The aim is to determine Φ_d from the measured flux Φ . Hence, it is necessary to invert Eq. (8) which is possible by using the W Lambert function. However, the correction function is commonly use in a different form. The Taylor expansion of Φ is

$$\Phi = \Phi_d e^{-\Phi_d \tau} = \Phi_d - \tau \Phi_d^2 + \Phi_d^3 \mathcal{E}(\Phi_d) \quad (9)$$

By noting that equation (9) is the Taylor expansion of

$$\frac{\Phi_d}{1 + \tau \Phi_d} = \Phi_d - \tau \Phi_d^2 + \Phi_d^3 \mathcal{E}(\Phi_d) \quad (10)$$

and that $\Phi_d \tau$ is small, one has

$$\Phi_d \simeq \frac{\Phi}{1 - \Phi} \quad (11)$$

$\Phi_d \tau$ is typically equal to 0.1. This induces a 0.44% relative error on the correction process.

4.3 Signal post-processing

The time evolution of the photon flux is expected to represent the time evolution of the density. An example of

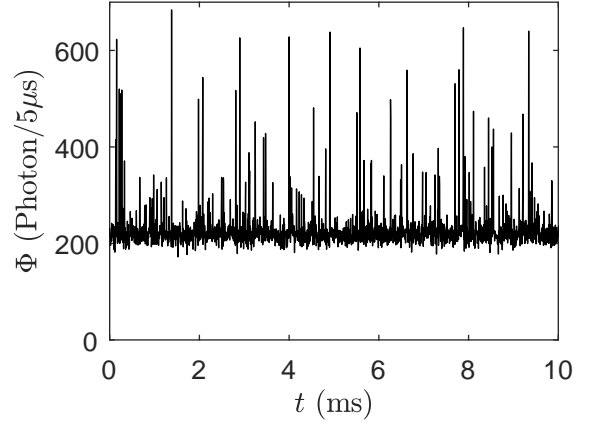


Figure 3: Photon flux sampled at 200 kHz measured on the centreline of a high speed jet.

a time history of this flux measured in a high speed jet is provided in Fig. 3. This plot is representative of all Rayleigh scattering records. It can be divided into four components. An average component linearly related to the average flow density, a fluctuating part related to density fluctuations, a fluctuating part induced by shot noise, and spikes corresponding to dust particles passing across the beam. Actually, the record is taken in the potential core the jet, where density fluctuations are very low, therefore the fluctuations visible in this graph are almost fully due to shot noise, and cannot be removed by signal processing. However, the dust spikes exhibit recognisable features, and their incidence on the density result can be distinctly reduced by post-processing.

The dust spike removing process takes advantage of mainly two features of these spikes: they all consist in an excess of photons, and they minimum time width can be estimated from the local speed of flow and from the beam diameter. They are also in general of high intensity, but due to the Gaussian shape of the beam, some particles may be lighted up by residual laser light close to the beam. For the same reason, the width of the spike can decrease if the particle does not pass through the center of the beam. The first step of the process is to estimate the required sampling frequency of the photon flux to ensure spikes are made of more than one sample. In fact in this case, clean signal can be hidden by the spike because the time resolution is not large enough. Since this frequency is defined, the signal is sampled thanks to the method described in Sec. 4.2. Then the histogram of the flux is calculated. The lower half part of the histogram is assumed not to be affected by spikes. Because shot noise is dominant, the shape of the half histogram is a half Gaussian curve from which is determined the standard deviation, and the average. A threshold is defined to be 2.5 standard deviation above the average, and all samples of values higher than the threshold are replace by a random number taken from a distribution of the same average and same standard deviation. The choice of replacing the corrupted samples by random signal will be justified in Sec 6.3 for the estimation of fluctuations. An

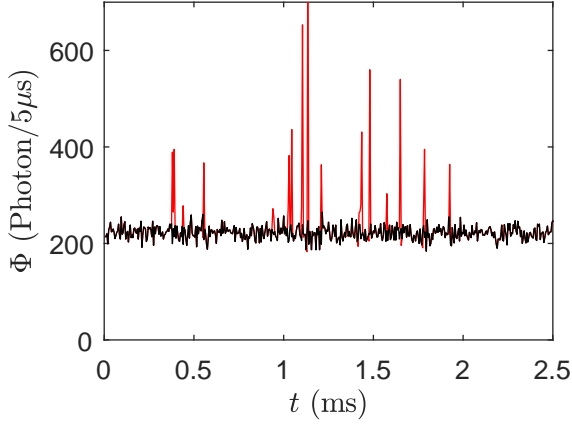


Figure 4: Post-processing dust spike removing effect. In red the raw signal, and in black the cleaned signal.

illustration of the efficiency of this signal cleaning process is presented in Fig. 4.

5. VALIDATION

The validation tests conducted to check if results are in accordance with theoretical behaviour predicted in Eq. (5) are now presented. Since the gas properties, the collection optic, the laser wave length, and the quantum efficiency of the sensor are fixed, the remaining variables are the laser intensity, the polarisation angle, and the density.

Another property to check is the Poissonian distribution of the photon flux. Contrary to the above-mentioned quantities proper to Rayleigh scattering, this test aims at assessing the counting method, but will not provide information about the nature of the collected light. Poisson distribution imposes the standard deviation of a variable to equals the square root of the mean value of the same variable. Here the variable is the number of photon per time window Δt , and it is expected that

$$\sigma_{\Phi_d \Delta t} = \sqrt{\overline{\Phi_d \Delta t}} \quad (12)$$

where $\sigma_{\Phi_d \Delta t}$ is the standard deviation of a flux sampled at f_{acq} , and the top bar represents the time average. These two quantities are computed from the flux signals obtained for different laser powers, sampled at 200 kHz during 0.8 s, and the linear relation between them is validated in Fig. 5. The photon-counting method is therefore considered valid.

The relation between the counted photon flux and the laser intensity is presented in Fig. 6(a). After the flux is corrected by considering a 2 ns pulse pair resolution, the expected linear dependency between these two quantities is well verified. However, an offset of 1.7×10^5 photon/s is measured while laser power is zero. This offset corresponds to the contribution of the stray light inside the anechoic room. The agreement between prediction of the flux at 5 W deduced theoretical point of view in Eq. (6), and the experimental measurement provides a strong con-

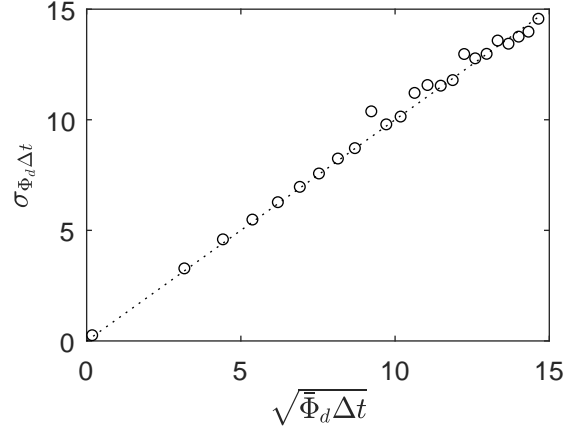


Figure 5: Standard deviation of a signal sampled at 200 kHz ($\Delta t = 5 \mu s$) against the square roots of the same signal

fidence with regard to the captured phenomenon. The measured flux is only 10% lower than the estimated flux.

The dependency of Φ_d to the polarisation angle ϕ is compared with theoretical behaviour in Fig. 6(b). Experimental data superimpose well on a \sin^2 shaped curve offsetted by flux similar with the laser off flux. This is also an argument confirming that the measured phenomenon is related to Rayleigh scattering, in fact, the scattering of larger particle is less dependent upon the polarisation angle [2].

The last validation concerns the relation between the collected flux, and the density. This required to control the density, which is not straightforward. Panda and Seasholtz [10] proposed a method taking advantage of compressibility effects in high speed jets. By assuming isentropic flow, the density ρ_j in the potential core of a jet can be related to the jet Mach number M_j if the total pressure P_0 , the ambient pressure P_{amb} , and the total temperature T_0 are known

$$\rho_j = \frac{P_0}{rT_0} \left(\frac{P_0}{P_{amb}} \right)^{-1/\gamma} \quad (13)$$

where r is the specific gas constant, and γ is the specific heat ratio. The wind tunnel apparatus allows for measuring all the required inputs, and the isentropic assumption is considered as true while $M_j < 1$, thus the photon flux is measured for several Mach number to provide the results shown in Fig. 7. This validation test also provides the constants of calibration a and b of the measuring bench. In fact, the linearity is experimentally observed, and relate ρ to Φ by

$$\rho = \frac{\Phi - b}{a} = \frac{\Phi - 1.7 \times 10^5}{3.3 \times 10^7} \quad (14)$$

Nevertheless, the measured quantity is not directly the flux but the number of photons per time window $N_i = \Phi_i \Delta t$ where i denote the i^{th} time window, and Φ_i is the average flux during this same time window. A time depend ρ_i is thus defined

$$\rho_i = \frac{N_i - 1.7 \times 10^5 \Delta t}{3.3 \times 10^7 \Delta t} \quad (15)$$

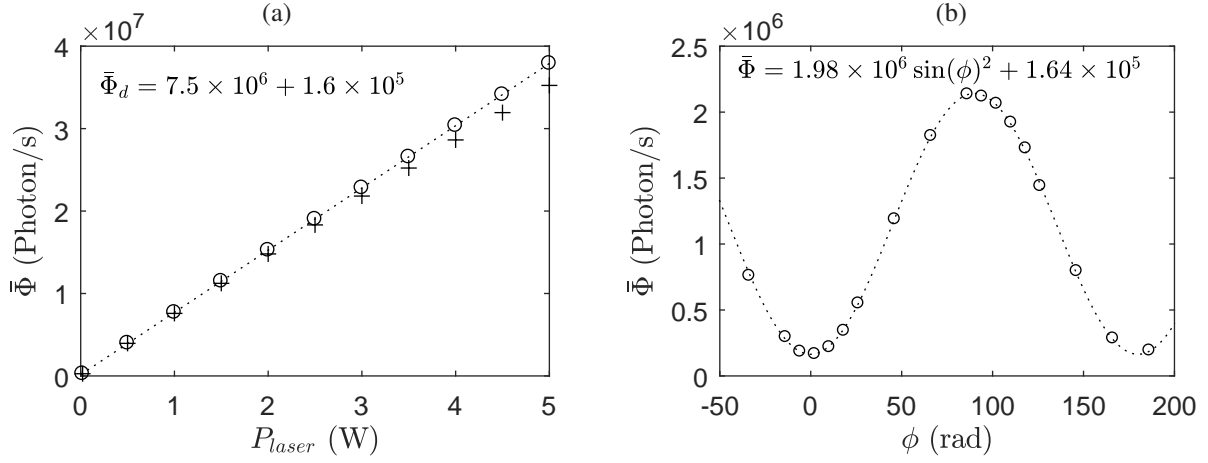


Figure 6: Validation of measurements obtained in air at $\rho = 1.2 \text{ kg/m}^3$. (a) the Photon flux is measured for various laser power. (b) the photon flux is measured for different polarisation angle at laser power 0.3 W. + counted flux, \circ corrected flux, \cdots best fitting curve.

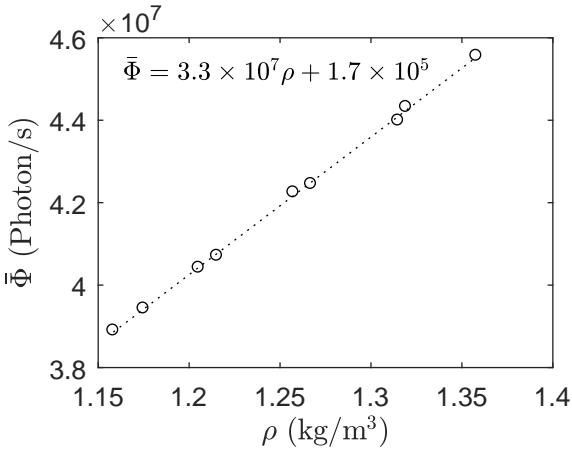


Figure 7: Calibration curve of the photon flux against the flow density.

6. MEASUREMENT

Profiles of density are measured in a Mach 0.9 round jet at 5 axial locations. The total temperature of the jet is 300 K and is exhausted into 289 K ambient air at an atmospheric pressure of 981 hPa. The nozzle diameter is $D = 38$ mm.

6.1 Time averaged

The mean density profiles are presented in Fig. 8 (a). Each point is calculated from a 0.8 s record of the photon flux turned into density according to the calibration given in Eq. (14). The profiles are compared with semi-empirical predictions based on the Crocco-busemann relation described in [10]. It is first worth noting that shapes of the measured and the predicted profiles are very similar. Nevertheless one may observe that profiles at $z/D = 2$ and 3 are just below the prediction, whereas others are slightly above. This is observed even outside the jet where temperature is directly measured, so where the uncertainties on density are the lowest. This discrepancies is most likely to be explained by a drift of calibration co-

efficient due for instance to a slow change of stray light incoming into the anechoic room.

6.2 Fluctuations

The root mean square fluctuations of the density are calculated from the root mean square fluctuation N'_{rms} of n samples of N_i

$$N'_{rms} = \frac{1}{n} \sum_{i=0}^{n-1} (N_i - \bar{N})^2 \quad (16)$$

with \bar{N} the mean value of N_i . Then, N'_{rms} can be converted in density fluctuations ρ'_{rms} with

$$\rho'_{rms} = \frac{N'_{rms}}{3.3 \times 10^7 \Delta t} \quad (17)$$

However, it is mentioned in the previous section that shot noise is a fluctuating contribution of variance equal to \bar{N} , which should be removed. The variance of N_i is the sum of the variances attributed to the shot noise $Var(N_{SN})$, and to the aerodynamic fluctuations $Var(N_a)$.

$$Var(N_i) = N'^2_{rms} = Var(N_{SN}) + Var(N_a) \quad (18)$$

But since $Var(N_{SN}) = \bar{N}$, and $Var(N_a) = N'^2_{a,rms}$, one has

$$N'_{a,rms} = \sqrt{N'^2_{rms} - \bar{N}} \quad (19)$$

and finally,

$$\rho'_{a,rms} = \frac{\sqrt{N'^2_{rms} - \bar{N}}}{3.3 \times 10^7 \Delta t} \quad (20)$$

The profiles of ρ'_{rms} and $\rho'_{a,rms}$ are presented in Fig. 8. There is a noticeable decrease of the fluctuating level consecutive to the shot noise removing. Nevertheless, there is still an unexpected level of fluctuations inside the potential core of the jet. Profiles at $z/D = 2, 3$, and 4 that cross the potential core exhibits the same level of about 0.04 kg/m^3 , that is to say about half the maximum level of fluctuation. Fluctuating velocities measured in the same

jet are found ten times lower in the potential core than in the shear layer. These spurious density fluctuation may be the consequence of water droplets that condensate inside the jet due to the expansion, and that would increase the number of particles crossing the laser beam.

6.3 Density fluctuation spectra

A classical mean to measure density fluctuation spectra is to apply the Welch's method on times series of the signal. Performing such an analysis to time history of photon flux would reveal the dominance of shot noise. This spurious white noise imposes a noise floor preventing from observing low level of fluctuations. This noise floor can be estimated by considering the shot noise as white noise. If the power spectral density of the shot noise is $P_{N_{SN}^2}$, then for Parseval identity

$$\int_0^{f_{acq}} P_{N_{SN}^2} df = Var(N_{SN}) \quad (21)$$

thus,

$$P_{N_{SN}^2} = 2 \frac{\bar{N}}{f_{acq}} \quad (22)$$

noting that

$$P_{\rho^2} = \left(\frac{f_{acq}}{a} \right)^2 P_{N^2} = \left(\frac{f_{acq} \bar{\rho}}{a \bar{\Phi}} \right)^2 P_{N^2} \quad (23)$$

The noise floor $P_{\rho_{SN}^2}$ is therefore given by

$$P_{\rho_{SN}^2} = \frac{2 \bar{\rho}^2}{\bar{\Phi}} = \frac{2 \bar{\rho}}{a} \quad (24)$$

6.3.1 Spectra from two photomultiplier signals

Panda and Seasholtz [11] proposed a method based on the use of two photomultipliers pointed toward the same flow region to vanish shot noise out. The two signals of counted photons are denoted N_1 and N_2 and are divided into m segments of length determined from the wanted frequency resolution, and that can overlap. They are denoted N_1^j and N_2^j with $j = 1, 2, 3, \dots, m$. The Fourier transform of each segment $F_{N_1^j}(f)$ and $F_{N_2^j}(f)$ is decomposed into a shot noise and an aerodynamic contribution

$$F_{N_1^j}(f) = F_{N_{1A}^j} + F_{N_{1SN}^j} \quad F_{N_2^j}(f) = F_{N_{2A}^j} + F_{N_{2SN}^j} \quad (25)$$

The one sided power density spectrum $P_{N_1 N_2}(f)$ is then calculated

$$P_{N_1 N_2}(f) = \frac{2}{m} \sum_{j=0}^{m-1} F_{N_1^j}(f) F_{N_2^j}^*(f) \quad (26)$$

where $*$ is the complex conjugate.

$$P_{N_1 N_2}(f) = \frac{2}{m} \sum_{j=0}^{m-1} F_{N_{1SN}^j} F_{N_{2SN}^j}^* + F_{N_{1A}^j} F_{N_{2A}^j}^* + F_{N_{1A}^j} F_{N_{2SN}^j}^* + F_{N_{1SN}^j} F_{N_{2A}^j}^* \quad (27)$$

Since shot noise related terms are random, the average of the product involving shot noise is zero, and if m is large enough, shot noise contribution can be neglected, so

$$|P_{N_1 N_2}(f)| \simeq |F_{N_{1A}^j} F_{N_{2A}^j}^*| \quad (28)$$

and

$$|P_{\rho^2}(f)| \simeq \frac{f_{acq}^2}{a_1 a_2} |P_{N_1 N_2}(f)| \quad (29)$$

where a_1 and a_2 are the calibration constants of the two collecting systems.

6.3.2 Spectra from one photomultiplier signal

If the sample rate is high enough in comparison with flow features, the hypothesis of frozen turbulence applies on the successive samples. The data-acquisition chain described in Sec. 4.1 is able to sample N_i at any rates up to few megahertz, and is therefore likely to meet the frozen turbulence hypothesis for many flows. A signal N_1 is generated from the odd index i , and a signal N_2 from the even index. The aerodynamic part of their respective Fourier transforms are therefore

$$F_{N_{2A}}(f) = F_{N_{1A}}(f) e^{-i \frac{2\pi f}{f_{acq}}} \quad (30)$$

while the shot noise parts are still independent of one another. The same reasoning applies as from two sensors, but the effective sampling frequency is $f_{acq}/2$ and the calibration constant is $a/2$.

6.3.3 Comparison of the two methods

The density fluctuation in two low Mach number flows characterised by two different temperature turbulent intensities are measured. Each configuration is measured with one, and two photomultipliers. The full records are made of thirty sub-record of 0.8 s sampled at 100 kHz for the single photomultiplier case, and 0.4 s per channel sampled at 50 kHz for the two photomultipliers case. The power density spectra of these two configurations are compared in Fig. 9. Whatever is the method, the first important point is the drop of more than one decade of the noise floor obtained from cross-spectra in comparison with a classical power density spectra estimation. Otherwise, no significant difference is observed between the results of both methods. The discrepancy observed at low frequency in Fig. 9(a) is most probably a drift of flow conditions during time spent for setting up the second configuration.

6.3.4 Estimation of the rms value

The reduction of the shot noise contribution in power density spectra by the computation of cross-spectra can be useful to estimate the rms value of the density fluctuation. From Parseval identity,

$$\rho'_{rms} = \sqrt{\int_0^{f_{acq}/2} |P_{\rho^2}(f)| df} \quad (31)$$

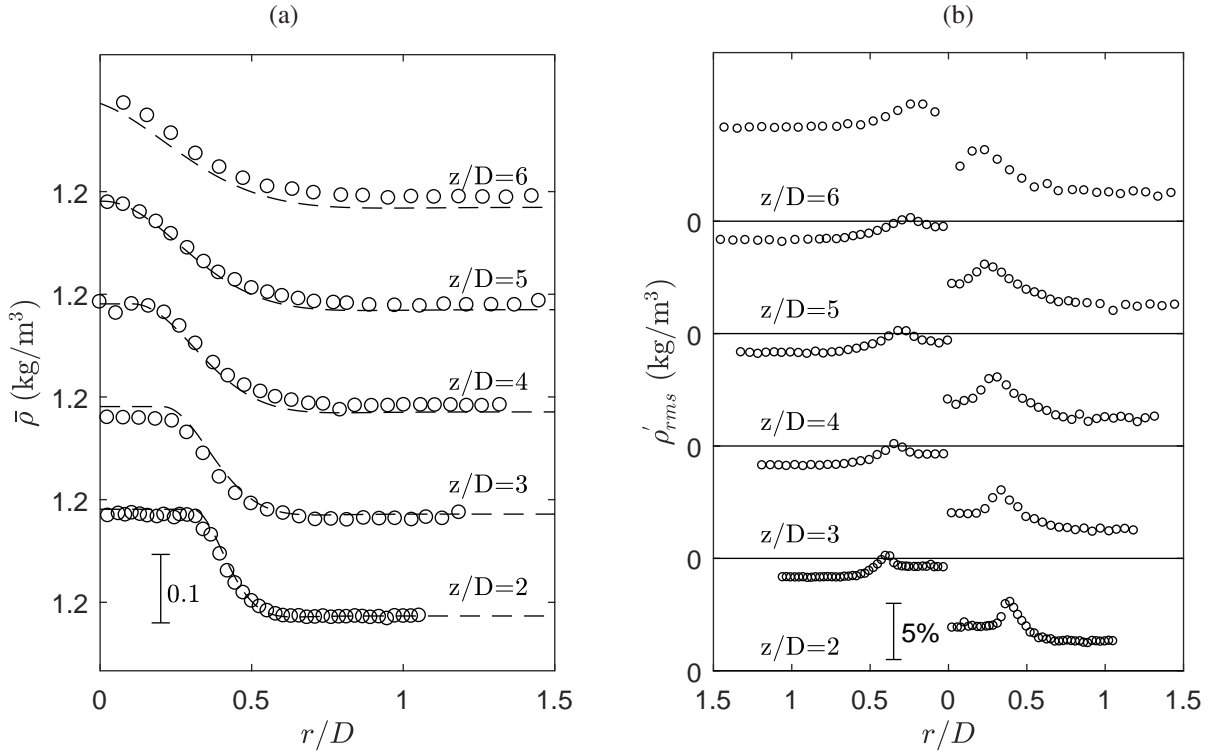


Figure 8: Density profiles measured in a $M_j = 0.9$ cold jet. (a) mean profiles. All profiles are shifted by 0.15 kg/m^3 for readability. — — — profile calculated from the Crocco-busemann relation [10]. (b) root means square fluctuations of the density. On the left side of this plot, fluctuations are measured directly from the photon flux, on the right side, the shot noise is removed. Profiles are shifted by 10% for readability.

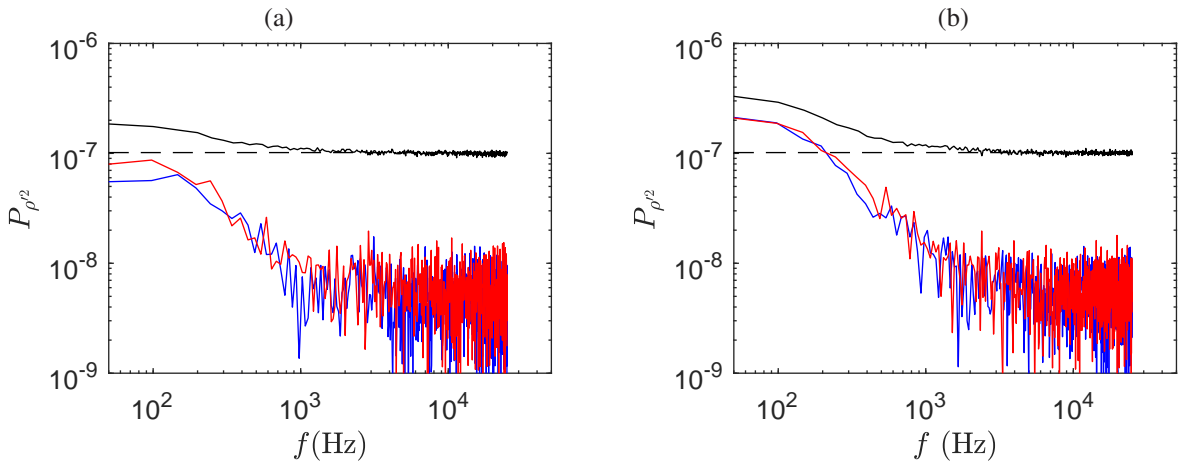


Figure 9: Power density spectra of the fluctuations calculated from one photomultiplier (in red) and two photomultiplier (in blue). The black spectra is calculated in a classical way from one photomultiplier, the dashed line is the associated theoretical noise floor. (a) low level of fluctuation flow, (b) higher level of fluctuation.

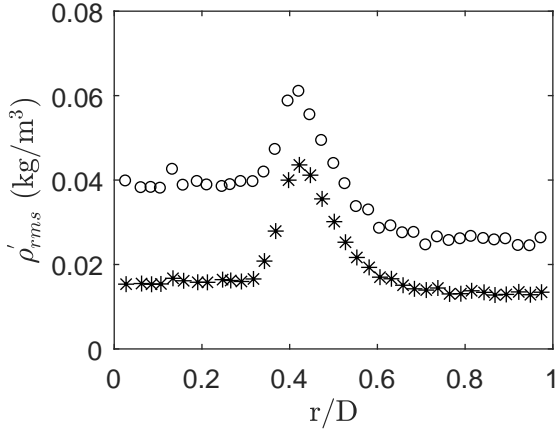


Figure 10: Density fluctuation profile at $z/D = 2$ in a $M_j = 0.9$ cold jet. \circ calculated from the photon flux fluctuation shot noise shortened, $*$ calculated by integrating the auto-spectra.

This integral is estimated by a trapezoidal integration of the computed discrete spectrum. The result of this process is shown in Fig. 10 and compared with the result obtained from Eq. 20 in the Mach 0.9 jet at $z/D = 2$. The level of fluctuations in the potential core, and in the no flow region is again decreased. This method is thus more efficient to remove shot noise contribution than a statistical approach.

7. CONCLUSION

A Rayleigh scattering based measurement system is set up. It differs from other systems mainly by the data acquisition method that is faster than traditional photon counters. The counted photon flux can therefore be increased, and so is the signal to noise ratio. A major source of noise of this measurement method is the presence of dust particles in flow. Their amount is decreased by filtering the flow, and a post processing method is described to reduce the adverse effect on the signal of the remaining particle detections.

Validation tests that are aimed to compare the experimental results to theoretical behaviour have been conducted. The experimental flux is found only 10% lower than the gross prediction. The expected linear dependency to the density and the laser power is also observed, as well as the direct link between the flux and the polarisation angle.

The method is applied on a Mach 0.9 jet. Mean density profiles are compared with profiles determined from the Crocco-Busemann relation. The comparison points out a good agreement, but the density seems to be slightly underestimated close to the nozzle, and become overestimated farther than $z/D = 4$. This discrepancy is most likely due to changes of calibration constants during the measuring process, and especially due to an offset introduced by stray light. Fluctuations profiles are also plotted to show how important it is to remove the shot noise contribution from these results. A statistical based method

is described to evaluate shot noise, but the most efficient way to reduce shot noise is to integrate the auto-spectrum of density fluctuations.

A new method of computing auto-spectrum based on one photomultiplier is compared with the method developed by Panda and Seasholtz [11] requiring two sensors. The comparison is performed in a low speed flow containing a significant amount of turbulent density intensity. Both methods are found to provide the same results.

All the results of this study show that setting up a Rayleigh scattering system is applicable to large facilities, and that the obtained results can provide insight into the compressible flow structures.

ACKNOWLEDGMENT

This work was performed within the framework of the Labex CeLyA of Université de Lyon, within the program “Investissements d’Avenir” (ANR-10-LABX-0060/ANR-11-IDEX-0007) operated by the French National Research Agency (ANR), and is also partially supported by the industrial Chair ADOPSYS co-financed by SAFRAN-SNECMA and ANR (ANR-13-CHIN-0001-01).

REFERENCES

- [1] Benoît André, Thomas Castelain, and Christophe Bailly. Investigation of the mixing layer of underexpanded supersonic jets by particle image velocimetry. *International Journal of Heat and Fluid Flow*, 50:188 – 200, 2014.
- [2] Craig F Bohren and Donald R Huffman. *Absorption and scattering of light by small particles*. Wiley, New York, 1983.
- [3] Vincent Fleury, Christophe Bailly, Emmanuel Jondeau, Marc Michard, and Daniel Juvé. Space-time correlations in two subsonic jets using dual particle image velocimetry measurements. *AIAA journal*, 46(10):2498–2509, 2008.
- [4] Franck Kerhervé, Peter Jordan, Yves Gervais, Jean-Christophe Valière, and Patrick Braud. Two-point laser doppler velocimetry measurements in a mach 1.2 cold supersonic jet for statistical aeroacoustic source model. *Experiments in fluids*, 37(3):419–437, 2004.
- [5] Amy F. Mielke and Kristie A. Elam. Dynamic measurement of temperature, velocity, and density in hot jets using rayleigh scattering. *Experiments in Fluids*, 47(4):673–688, 2009.
- [6] Amy F Mielke-Fagan, Michelle M Clem, and Kristie A Elam. Rayleigh scattering measurements using a tunable liquid crystal fabry-perot interferometer. *AIAA paper*, 4350-2010.

- [7] Richard B Miles, Walter R Lempert, and Joseph N Forkey. Laser rayleigh scattering. *Measurement Science and Technology*, 12(5):R33, 2001.
- [8] Jayanta Panda. Experimental investigation of turbulent density fluctuations and noise generation from heated jets. *Journal of Fluid Mechanics*, 591:73–96, 2007.
- [9] Jayanta Panda. A molecular rayleigh scattering setup to measure density fluctuations in thermal boundary layers. *Experiments in Fluids*, 57(12):183, 2016.
- [10] Jayanta Panda and Richard G Seasholtz. Density measurement in underexpanded supersonic jets using rayleigh scattering. *AIAA paper*, 1998-281.
- [11] Jayanta Panda and Richard G Seasholtz. Experimental investigation of density fluctuations in high-speed jets and correlation with generated noise. *Journal of Fluid Mechanics*, 450:97–130, 2002.
- [12] Jayanta Panda, Richard G Seasholtz, and Kristie A Elam. Investigation of noise sources in high-speed jets via correlation measurements. *Journal of Fluid Mechanics*, 537:349–385, 2005.
- [13] Cecilia D. Richards and William M. Pitts. Global density effects on the self-preservation behaviour of turbulent free jets. *Journal of Fluid Mechanics*, 254:417–435, 009 1993.
- [14] Martin J. Schaffar. Direct measurements of the correlation between axial in-jet velocity fluctuations and far field noise near the axis of a cold jet. *Journal of Sound and Vibration*, 64(1):73–83, 1979.
- [15] Richard G Seasholtz, Alvin E Buggele, and Mark F Reeder. Flow measurements based on rayleigh scattering and fabry-perot interferometer. *Optics and lasers in engineering*, 27(6):543–570, 1997.
- [16] Richard G Seasholtz and Jayanta Panda. Multiple point dynamic gas density measurements using molecular rayleigh scattering. In *18th ICIASF*, pages 43/1–4310, 1999.
- [17] Richard G Seasholtz, Jayanta Panda, and Kristie A Elam. Rayleigh scattering diagnostic for measurement of velocity and density fluctuation spectra. *AIAA paper*, 2002-827.
- [18] Andrew T Young. Rayleigh scattering. *Physics Today*, 35(1):42–48, 1982.